AIAA 80-0125R

Propeller Slipstream/Wing Interaction in the Transonic Regime

M. H. Rizk*
Flow Research Company, Kent, Wash.

The purpose of this paper is to present a new approach to the propeller slipstream/wing interaction problem in the transonic regime. Approximations consistent with the physical problem of a nearly uniform slipstream interacting with a thin wing allow the perturbation velocities due to the interaction to be potential although the undisturbed slipstream is rotational. The resulting boundary-value problem is solved by standard finite-difference schemes for transonic potential flows. The approach presented here overcomes the deficiencies of panel methods which fail to correctly predict solutions in supersonic patches and at shock waves. The advantages of the present approach over solving the Euler equations include its relative simplicity, small computer storage requirements, and short computational time. The basic characteristics of the slipstream/wing interaction are demonstrated through simple numerical examples. They indicate that the slipstream has a strong effect on the aerodynamic properties of the wing section within the slipstream and lesser effects elsewhere. The slipstream swirling motion strongly affects the wing load distribution; however, its effect on the wing's total lift and wave drag is small. The axial velocity increment in the slipstream has a small effect on the wing lift; however, it causes a large increase in wave drag.

Nomenclature

a = speed of sound
c_l = section lift coefficient
h = enthalpy
M = Mach number
p = pressure
q = perturbation velocity vector
Q = velocity vector
Q = flow speed
r = radial coordinate
R = radial coordinate of slipstream boundary
S = deviation of the wing surface from a horizontal plane
u = perturbation velocity component in the z direction
U = velocity component in the z direction
ΔU = deviation of U from its average value
v = perturbation velocity component in the r direction
V = velocity component in the r direction
w = perturbation velocity component in the θ direction
W = velocity component in the θ direction
z = axial coordinate
α = $1/U_{i\infty}(R_\infty)$
α_s = slipstream swirl angle
β = $\alpha M^2_{o\infty} a^2_{i\infty}(R_\infty)$
γ = ratio of specific heats
ζ = vorticity vector
η = deviation of slipstream boundary from its undisturbed position
θ = angular coordinate
μ = $\max\{0, [1-(a^2/Q^2)]\}$
ξ_r = stretching factor in r direction
ξ_z = stretching factor in z direction
ξ_θ = stretching factor in θ direction
ρ = density
ϕ = perturbation velocity potential
ψ = undisturbed radius of a streamline

Subscripts

i = inner region variables
o = outer region variables
t = total conditions
∞ = undisturbed conditions

Superscript

$(\bar{\ })$ = average quantity

Introduction

INTEREST in turboprop propulsion systems has been recently revived due to the propulsion efficiency of these systems and the predicted fuel shortages in the future. Propeller slipstreams will interact with wings causing changes in their aerodynamic properties. The determination of the effects of slipstream/wing interaction is therefore necessary before any design decisions regarding the installation of turboprop propulsion systems can be derived. Since current passenger flight cruise speeds are in the transonic range, this is the range considered here.

The interaction of wings with regions of high-energy flow embedded in uniform streams was studied by Shollenberger,[1] who used flow singularities to simulate a jet interacting with a wing. The flow solution and jet position were found by calculating the singularity strengths and locations. Lan[2] used a quasi vortex-lattice method and a two-vortex-sheet representation of the slipstream to study the interaction problem with different slipstream and freestream Mach numbers. Ting et al.[3] used the method of asymptotic expansions to study the interference of a wing with multipropellers. The effect of nonuniform streams on the aerodynamic characteristics of wings have been studied by Chow et al.[4] and Kleinstein and Liu.[5] Boctor et al.[6] have recently studied the interaction of the slipstream with a wing-body configuration at high subsonic Mach numbers, using the panel method. This method does not include treatment of local patches of supersonic flow and shock waves. Therefore, though it may indicate qualitative trends, it fails to give quantitative descriptions of flows in the transonic regime. In addition to the theoretical studies mentioned above, experimental tests were conducted by Welge and Crowder[7] to assess the magnitude of the aerodynamic interference of a propeller slipstream on a supercritical wing.

Presented as Paper 80-0125 at the AIAA 18th Aerospace Sciences Meeting, Pasadena, Calif., Jan. 14-16, 1980; submitted Feb. 11, 1980; revision received June 24, 1980.

*Research Scientist. Member AIAA.

Except for the final experimental study, all previous studies dealing with slipstream/wing interaction are limited to subsonic flows. In this paper we use a simplified model to describe the interaction between a propeller slipstream and a wing in the transonic regime. The undisturbed slipstream boundary is assumed to coincide with an infinite circular cylinder. The undisturbed slipstream velocity is rotational and is a function of the radius only. In general, the velocity perturbation caused by introducing a wing into the slipstream is also rotational. By making small disturbance assumptions, however, the perturbation velocity becomes nearly potential and an approximation for the flow is obtained by solving a potential equation. This simplified model allows us to obtain basic information about the interaction problem while avoiding the need for solving the more complex Euler equations.

Formulation and Governing Equations

The present analysis considers a wing in a flow with a slipstream (inner flow region) embedded in a freestream (outer flow region). Far upstream of the wing, flow conditions are undisturbed by the wing. There the freestream Mach number is $M_{o\infty}$, and the slipstream is a circular cylinder of radius R_∞ with total enthalpy $h_{ti\infty}(r)$ and velocity distribution $\boldsymbol{Q}_i = [U_{i\infty}(r),\ 0,\ W_{i\infty}(r)]$. The flow velocities and the enthalpy are normalized here by the freestream flow speed and the square of the freestream flow speed, respectively. The cylindrical coordinates (z,r,θ) are used, with the z axis coinciding with the axis of the undisturbed slipstream. We use subscripts i, o, ∞, and t to denote inner region properties, outer region properties, undisturbed conditions, and total conditions, respectively. As the wing is approached, the flow is perturbed from its basic undisturbed condition. Since the flow is potential in the outer flow region, we may express the velocity perturbation there as $\boldsymbol{q}_o = \nabla\phi_o$. In the slipstream, the flow is rotational in general and we let $\boldsymbol{q}_i = (u_i, v_i, w_i)$ be the velocity perturbation there. Due to the wing effect the slipstream boundary deviates from the undisturbed circular cylinder and is defined by

$$r = R(z,\theta) = R_\infty + \eta(z,\theta)$$

where η is the amount of deviation from the undisturbed position.

The conditions at the interface specifying zero normal flow to it are

$$v_i = U_i\eta_z + W_i\frac{\eta_\theta}{R}, \qquad r=R \tag{1}$$

$$\phi_{or} = U_o\eta_z + W_o\frac{\eta_\theta}{R}, \qquad r=R \tag{2}$$

and the condition specifying zero pressure jump across the interface is

$$\frac{Q_i^2 - Q_{i\infty}^2}{Q_o^2 - 1} = M_{o\infty}^2 a_{i\infty}^2 \tag{3}$$

where Q is the magnitude of the velocity $\boldsymbol{Q}$, and a is the sound speed normalized by the freestream flow speed. The continuity equation is

$$\nabla\cdot(\rho\boldsymbol{Q}) = 0 \tag{4}$$

or

$$\frac{\partial}{\partial z}(\rho U) + \frac{1}{r}\frac{\partial}{\partial r}(r\rho V) + \frac{1}{r}\frac{\partial}{\partial\theta}(\rho W) = 0$$

where ρ, the density normalized by the freestream density, is given by

$$\rho(z,r,\theta) = \rho_\infty(\psi)\left\{1 + \frac{\gamma-1}{2}M_\infty^2(\psi)\left[1 - \frac{Q^2(z,r,\theta)}{Q_\infty^2(\psi)}\right]\right\}^{1/(\gamma-1)} \tag{5}$$

γ is the ratio of specific heats, and $\psi(z,r,\theta)$ the radius of the streamline passing through point (z,r,θ) in the undisturbed flow region far upstream of the wing. In general, the velocity perturbation inside the slipstream is rotational, and a complete solution requires solving the continuity equation (4) in addition to the Euler equation

$$(\boldsymbol{Q}\cdot\nabla)\boldsymbol{Q} = -\frac{1}{\rho}\nabla p, \qquad r<R \tag{6}$$

inside the slipstream, solving the continuity equation outside the slipstream, and determining the slipstream boundary $R(z,\theta)$.

Small Perturbation Approximation

We introduce here two simplifying assumptions under which the requirement for solving Euler's equation in the inner region is dropped. The first assumption is that the undisturbed inner region flow is nearly uniform,

$$\frac{\sqrt{W_{i\infty}^2(r) + \Delta U_{i\infty}^2(r)}}{\bar{U}_{i\infty}} \ll 1$$

where

$$U_{i\infty}(r) = \bar{U}_{i\infty} + \Delta U_{i\infty}(r)$$

and $\bar{U}_{i\infty}$ is the average value of $U_{i\infty}(r)$. The second assumption we introduce is the small disturbance assumption which limits us to wings with small surface slopes. To see the simplifying effects of these assumptions we take the curl of Eq. (6). This gives

$$(\boldsymbol{Q}\cdot\nabla)\zeta = \frac{\zeta}{\rho}(\boldsymbol{Q}\cdot\nabla)\rho + (\zeta\cdot\nabla)\boldsymbol{Q} + \frac{1}{\rho^2}(\nabla\rho\times\nabla p) \tag{7}$$

for $r<R$, where ζ is the vorticity,

$$\zeta = \nabla\times\boldsymbol{Q}$$

Under the two assumptions made above, Eq. (7) to lowest order becomes

$$\frac{\partial\zeta}{\partial z} = 0$$

This allows us to express the velocity perturbation in the inner region in terms of a velocity potential and the governing equations simplify to

$$\frac{\partial}{\partial z}\left[\rho(U_\infty + \phi_z)\right] + \frac{1}{r}\frac{\partial}{\partial r}(r\rho\phi_r) + \frac{1}{r}\frac{\partial}{\partial\theta}\left[\rho\left(W_\infty + \frac{1}{r}\phi_\theta\right)\right] = 0$$

where

$$U_\infty = \begin{cases} U_{i\infty}(r) & r<R_\infty \\ 1 & r>R_\infty \end{cases}$$

$$W_\infty = \begin{cases} W_{i\infty}(r) & r<R_\infty \\ 0 & r>R_\infty \end{cases}$$

and ρ is given by Eq. (5) with ψ replaced by r. The governing equation is further simplified through replacing the full-

potential equation by the transonic small disturbance equation

$$\frac{\partial}{\partial z}\left[\rho(U_\infty+\phi_z)\right]+\frac{1}{r}\frac{\partial}{\partial r}(r\rho_\infty\phi_r)+\frac{1}{r}\frac{\partial}{\partial\theta}\left(\frac{1}{r}\rho_\infty\phi_\theta\right)=0 \quad (8)$$

where ρ is to be approximated by the first four terms of the binomial expansion for Eq. (5). The conditions at the slipstream boundary reduce to

$$\frac{\phi_r(z,R_\infty-\epsilon,\theta)}{\phi_r(z,R_\infty+\epsilon,\theta)}=U_{i\infty}(R_\infty) \qquad \epsilon\to 0 \quad (9)$$

and

$$\frac{\phi_z(z,R_\infty-\epsilon,\theta)}{\phi_z(z,R_\infty+\epsilon,\theta)}=\frac{M_{\infty\infty}^2 a_{i\infty}^2(R_\infty)}{U_{i\infty}(R_\infty)} \qquad \epsilon\to 0 \quad (10)$$

Numerical Approach

Computational Mesh

The solution to the governing equations is found numerically. We therefore define a net of discrete points (z^i,r^j,θ^k) in the computational domain, with

$$0\le i\le I+1, \quad 1\le j\le J+1, \quad 1\le k\le K$$

The computational domain is bounded by an outer cylindrical boundary $(r=r^{J+1})$, an upstream vertical plane $(z=z^0)$, and a downstream vertical plane $(z=z^{I+1})$. The undisturbed cylindrical slipstream boundary $(r=R_\infty)$ lies between the two cylindrical mesh surfaces $r=r^{j_s-1}$ and $r=r^{j_s}$, $j=j_s$, such that

$$R_\infty=(r^{j_s-1}+r^{j_s})/2$$

The wing lies in the horizontal plane passing through the slipstream axis. (See Fig. 1.)

A computational mesh with nonuniform spacings in the θ direction and with a stretching factor

$$\xi_\theta=\frac{\theta^k-\theta^{k-1}}{\theta^{k+1}-\theta^k}, \qquad 0<\theta<\frac{\pi}{2}$$

is used. The mesh is symmetric about both the horizontal and vertical planes. Inside a cylindrical region with an axis coinciding with the z axis and with its surface and end planes containing the outermost wing tips, the mesh spacings in both the axial and radial directions are uniform. Outside this cylinder, however, the mesh spacings increase as the outer boundaries are approached. The stretching factors in the axial and radial directions are ξ_z and ξ_r, respectively.

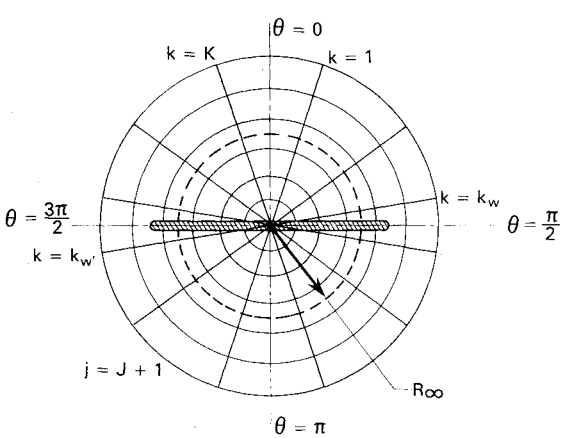

Fig. 1 Cross section through computational mesh at constant z plane.

Finite-Difference Formulas

The finite-difference approximation to the governing equation (8) at point (z^i,r^j,θ^k), where $1\le i\le I$, $2\le j\le J$, and $1\le k\le K$ is

$$\frac{(\tilde\rho U)^{i+\frac12,j,k}-(\tilde\rho U)^{i-\frac12,j,k}}{z^{i+\frac12}-z^{i-\frac12}}+\frac{1}{r^j}\frac{(\rho_\infty rV)^{i,j+\frac12,k}-(\rho_\infty rV)^{i,j-\frac12,k}}{r^{j+\frac12}-r^{j-\frac12}}+\frac{1}{r^j}\frac{(\rho_\infty W)^{i,j,k+\frac12}-(\rho_\infty W)^{i,j,k-\frac12}}{\theta^{k+\frac12}-\theta^{k-\frac12}}=0 \quad (11)$$

where

$$(\tilde\rho U)^{i+\frac12,j,k}=\tilde\rho^{i+\frac12,j,k}U^{i+\frac12,j,k}$$

with similar definitions for the other bracketed terms, and where

$$U^{i,j,k}=U_\infty(r^j)+u^{i,j,k}$$

$$V^{i,j,k}=v^{i,j,k}$$

$$W^{i,j,k}=W_\infty(r^j)+w^{i,j,k}$$

Here $U^{i,j,k}$, $V^{i,j,k}$, and $W^{i,j,k}$ denote approximations to the velocity components at point (z^i,r^j,θ^k). The modified density, $\tilde\rho^{i+\frac12,j,k}$, is given by

$$\tilde\rho^{i+\frac12,j,k}=\rho^{i+\frac12,j,k}+\Delta\rho^{i+\frac12,j,k}$$

$$\Delta\rho^{i+\frac12,j,k}=-\mu^{\hat\imath,j,k}(\rho^{i+\frac12,j,k}-\rho^{i-\frac12,j,k}) \quad (12)$$

where

$$\hat\imath=\begin{cases} i & \mu^{i+2}=0 \\ i+\frac12 & \mu^{i+2}\ne 0\end{cases}$$

and the switching function μ is given by

$$\mu=\max\left[0,\left(1-\frac{a^2}{Q^2}\right)\right]$$

The artificial viscosity

$$T^{i,j,k}=\frac{(\Delta\rho^{i+\frac12,j,k}U^{i+\frac12,j,k})-(\Delta\rho^{i-\frac12,j,k}U^{i-\frac12,j,k})}{z^{i+\frac12}-z^{i-\frac12}}$$

is an approximation to

$$-\frac{\partial}{\partial z}(U\mu\rho_z\Delta z)$$

(where Δz is the mesh spacing in the z direction). This viscosity has been added to the central difference approximation to Eq. (8) in order to produce a stable difference scheme in the supersonic zone. This form for the viscosity was introduced by Jameson[8] to solve the full-potential equation in conservative form. Since the flow is nearly aligned with the z coordinate, it is sufficient to add the viscosity to the z derivative only.

The perturbation velocity components $u^{i+\frac{1}{2},j,k}$ and $u^{i-\frac{1}{2},j,k}$ are defined by the formula

$$u^{i\pm\frac{1}{2},j,k}=\frac{\phi^{i\pm1,j,k}-\phi^{i,j,k}}{z^{i\pm1}-z^{i}}$$

Similar formulas for $v^{i,j+\frac{1}{2},k}$ and $v^{i,j-\frac{1}{2},k}$ are used at all mesh points except those at the slipstream boundary where $j=j_s-1$ and $j=j_s$, respectively.

Expressions for the radial velocity components $v-^{i,k}$ and $v+^{i,k}$ at the slipstream boundary in the inner and outer regions, respectively, are found in terms of the potentials $\phi^{i,j,k}$ and $\phi^{i,j-1,k}$, $j=j_s$ as follows. We define a fictitious potential $\Phi^{i,k}$ at point (z^i,r^j,θ^k), $j=j_s$, so that

$$v-^{i,k}=\frac{\Phi^{i,k}-\phi^{i,j-1,k}}{r^j-r^{j-1}},\qquad j=j_s \tag{13}$$

and it follows from Eq. (9) that

$$v+^{i,k}=\alpha\frac{\Phi^{i,k}-\phi^{i,j-1,k}}{r^j-r^{j-1}},\qquad j=j_s \tag{14}$$

where

$$\alpha=\frac{1}{U_{i\infty}(R_\infty)}$$

We may now express the axial velocity perturbation components $u-^{i-\frac{1}{2},k}$ in the inner region at the slipstream boundary and $u+^{i-\frac{1}{2},k}$ in the outer region at the slipstream boundary as follows

$$u-^{i-\frac{1}{2},k}=\{[\Phi^{i,k}-\tfrac{1}{2}v-^{i,k}(r^j-r^{j-1})]-[\Phi^{i-1,k}-\tfrac{1}{2}v-^{i-1,k}(r^j-r^{j-1})]\}/(r^j-r^{j-1}),\qquad j=j_s$$

and

$$u+^{i-\frac{1}{2},k}=\{[\phi^{i,j,k}-\tfrac{1}{2}v+^{i,k}(r^j-r^{j-1})]-[\phi^{i-1,j,k}-\tfrac{1}{2}v+^{i-1,k}(r^j-r^{j-1})]\}/(r^j-r^{j-1}),\qquad j=j_s$$

Substituting the expressions for $u-^{i-\frac{1}{2},k}$ and $u+^{i-\frac{1}{2},k}$ into Eq. (10) leads to an expression for $\Phi^{i,k}$. When substituted into Eqs. (13) and (14) this leads to the expressions

$$v^{i,(j-1)+\frac{1}{2},k}=\frac{2(\beta\phi^{i,j,k}-\phi^{i,j-1,k})}{(r^j-r^{j-1})(1+\alpha\beta)},\qquad j=j_s \tag{15}$$

for points in the inner region at the slipstream boundary, and

$$v^{i,j-\frac{1}{2},k}=\frac{2\alpha(\beta\phi^{i,j,k}-\phi^{i,j-1,k})}{(r^j-r^{j-1})(1+\alpha\beta)},\qquad j=j_s \tag{16}$$

for points in the outer region at the slipstream boundary, where

$$\beta=\alpha M^2_{o\infty}a^2_{i\infty}(R_\infty)$$

The perturbation velocity components $w^{i,j,k+\frac{1}{2}}$, $w^{i,j,k-\frac{1}{2}}$ are defined by the formula

$$w^{i,j,k\pm\frac{1}{2}}=\frac{1}{r^j}\frac{\phi^{i,j,k\pm1}-\phi^{i,j,k}}{\theta^{k\pm1}-\theta^k}$$

at all points except those on the wing surface, and those in the wing wake. On the wing surface we use the small-disturbance boundary condition

$$w=U_\infty\left(\frac{\partial S}{\partial x}-\frac{W_\infty(r)}{U_\infty(r)}\right) \tag{17}$$

where S is the deviation of the wing surface from a horizontal plane and is defined to be positive in the direction of increasing θ. The potential function ϕ is discontinuous at the wing wake. There the following formulas are used

$$w^{i,j,k+\frac{1}{2}}=\frac{1}{r^j}\frac{\phi^{i,j,k+1}+G^j-\phi^{i,j,k}}{\theta^{k+1}-\theta^k}\qquad k=k_w,k_{w'}$$

$$w^{i,j,k-\frac{1}{2}}=\frac{1}{r^j}\frac{\phi^{i,j,k}-(\phi^{i,j,k-1}-G^j)}{\theta^k-\theta^{k-1}}\qquad k=k_w+1,k_{w'}+1$$

where

$$G^j=\begin{cases}C^j=\phi^j_{u,(\pi/2)}-\phi^j_{l,(\pi/2)}\\ -C'^j=-(\phi^j_{u,(3\pi/2)}-\phi^j_{l,(3\pi/2)})\end{cases}$$

and $\phi^j_{u,\Psi}$, $\phi^j_{l,\Psi}$ are, respectively, the values of the potential ϕ at the upper and lower surfaces of the wing trailing edge located at $\theta=\Psi$, $r=r^j$.

The far-field boundary conditions are given by

$$u^{0,j,k}=0\qquad \phi^{i,J+1,k}=0$$

and on the downstream plane ($z=z^{I+1}$) Eq. (11) is solved with the z derivative in that equation set equal to zero.

Finite-Difference Formulas at the Axis

We define a Cartesian coordinate system (x,y,z) with a horizontal x axis ($\theta=\pi/2$) and a vertical y axis ($\theta=0$). The continuity equation in Cartesian coordinates is

$$\frac{\partial}{\partial z}\left[\rho(U_\infty+\phi_z)\right]+\frac{\partial}{\partial x}(\rho_\infty\phi_x)+\frac{\partial}{\partial y}(\rho_\infty\phi_y)=0 \tag{18}$$

The finite-difference approximation to Eq. (18) is used for points along the z axis and is given by

$$\frac{(\tilde\rho U)^{i+\frac{1}{2},j,k}-(\tilde\rho U)^{i-\frac{1}{2},j,k}}{z^{i+\frac{1}{2}}-z^{i-\frac{1}{2}}}+\frac{(\rho_\infty V_c)^{i,j+\frac{1}{2},k_w+\frac{1}{2}}-(\rho_\infty V_c)^{i,j+\frac{1}{2},k_{w'}+\frac{1}{2}}}{\Delta x}+\frac{(\rho_\infty W_c)^{i,j+\frac{1}{2},T}-(\rho_\infty W_c)^{i,j+\frac{1}{2},B}}{\Delta y}=0 \tag{19}$$

where

$$V_c=\phi_x$$

$$W_c=\phi_y$$

$$(\ )^{i,j+\frac{1}{2},T}=\tfrac{1}{2}[(\ )^{i,j+\frac{1}{2},k_w}+(\ )^{i,j+\frac{1}{2},k_{w'}+1}]$$

$$(\ )^{i,j+\frac{1}{2},B}=\tfrac{1}{2}[(\ )^{i,j+\frac{1}{2},k_w+1}+(\ )^{i,j+\frac{1}{2},k_{w'}}]$$

and Δx, Δy are the mesh spacings in the x and y directions, respectively. The potential function ϕ is double valued at the axis. As the axis is approached from above, it takes a value ϕ^+ and, as it is approached from below, it takes another

value ϕ^-. We may therefore set

$$\begin{aligned}\phi^{i,1,k} &= \phi^{i+} \quad 0<\theta_k<\pi/2\\ &= \phi^{i-} \quad \pi/2<\theta_k<3\pi/2\\ &= \phi^{i+} \quad 3\pi/2<\theta_k<2\pi\end{aligned}$$

and we express the velocity components U, V_c, and W_c in terms of the potential function ϕ by formulas similar to those used for mesh points away from the axis.

Iterative Procedure

Equation (11) written at all mesh points off the axis and Eq. (19) written for all mesh points on the axis constitute a nonlinear system of algebraic equations for the potential function $\phi^{i,j,k}$ at the mesh points. Hafez et al.[9] recently solved the transonic full-potential equation by a simple line relaxation scheme which requires no special treatment for supersonic points. This simple scheme is used here. Before the nth iterative sweep through the computational domain, the values of $\tilde{\rho}$ are evaluated using the ϕ_{n-1} values obtained from the $n-1$ iterative sweep. Successive line overrelaxation is used along horizontal lines, so that the iterative solutions

$$\phi_n^{i,j,k}$$

at mesh points of constant r and θ values are obtained simultaneously. This involves solving linear systems of algebraic equations

$$A_{n-1}^{j,k}\phi_n^{i,k} = f_{n,n-1}^{j,k} \quad \begin{matrix} j=1,2,\ldots,J \\ k=1,2,\ldots,K \end{matrix}$$

where the coefficient matrix $A_{n-1}^{k,j}$ is a tridiagonal matrix. The nth iterative solution is given by

$$\phi_n^{i,j,k} = \phi_{n-1}^{i,j,k} + \omega(\phi_n^{i,j,k} - \phi_{n-1}^{i,j,k})$$

where ω is a relaxation factor. The sweeping is done for lines with $k=1$ to $k=K$ on a cylindrical surface, and is then continued for cylinders with increasing radii. At the end of the relaxation sweep the jump in potential at the wing trailing edge

$$G_n^j$$

is found and the nth iterative value is defined by the relation

$$G_n^j = G_{n-1}^j + \Omega(G_n^j - G_{n-1}^j)$$

where Ω is a relaxation factor. Relaxation sweeps of the computational domain are repeated until convergence occurs. In order to improve stability and the rate of convergence, a ϕ_{zt} term

$$-\kappa\frac{\tilde{\rho}_{n-1}^{i-\frac{1}{2},j,k}}{2}\frac{(\phi_n^{i,j,k}-\phi_{n-1}^{i,j,k})-(\phi_n^{i-1,j,k}-\phi_{n-1}^{i-1,j,k})}{(z_i-z_{i-1})\Delta t}$$

is added in the nth iterative sweep to the left-hand side of the algebraic equation solved for the mesh point (i,j,k) where κ is a constant and we set

$$\Delta t = z_i - z_{i-1}$$

Results and Discussion

The method presented above is used to demonstrate the slipstream effects through a simple numerical example. Results are calculated for a rectangular wing with NACA 0012 airfoil sections, and a 3 deg angle of attack. A freestream Mach number $M_{o\infty}=0.8$ is used. The wing planform is shown in Fig. 2. The slipstream swirl angle α_s and total pressure $p_{t\infty}$ distributions of highly loaded propellers currently under development (see Welge, et al.[7]) are shown in Figs. 3 and 4. We use these distributions in our calculations with a maximum swirl angle $\alpha_{s\infty\max}$ value of 3 deg. The calculations are carried out on a $49\times20\times24$ (z,r,θ) mesh, with 14 mesh points along the wing chord and 20 points along the wing span. The computational mesh extends 1.5 chord lengths upstream of the wing leading edge, 5 chord lengths downstream of the wing trailing edge, and the outer cylindrical computation mesh boundary radius is 4 chord lengths.

We note here that Eqs. (15) and (16) are valid for general α and β values. However, for the $p_{t\infty}/p_{to\infty}$ distribution of Fig. 4 both α and β are approximately unity. In this case it is consistent with the small-disturbance approximation to set

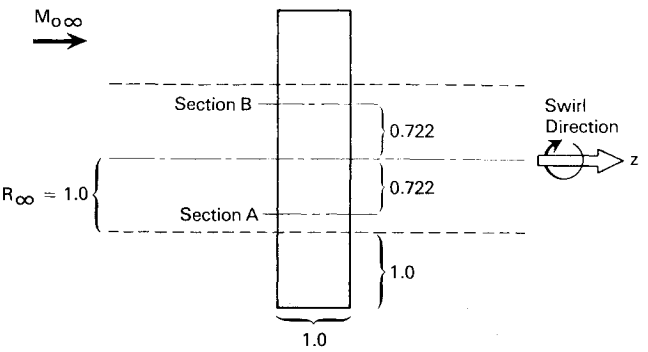

Fig. 2 Wing planform.

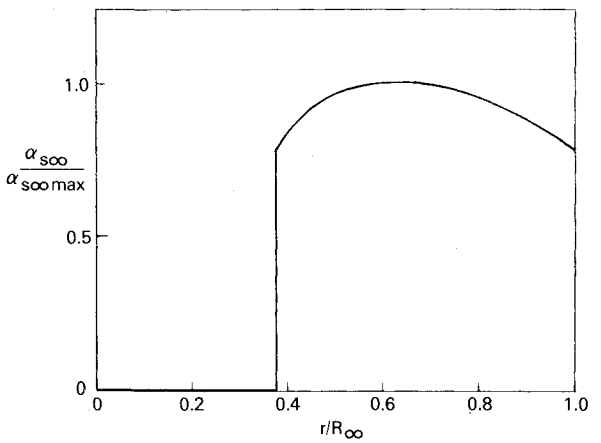

Fig. 3 Swirl angle distribution in undisturbed slipstream.

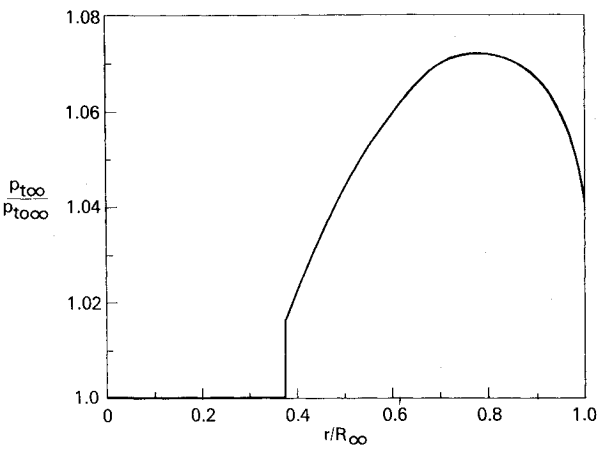

Fig. 4 Total pressure distribution in undisturbed slipstream.

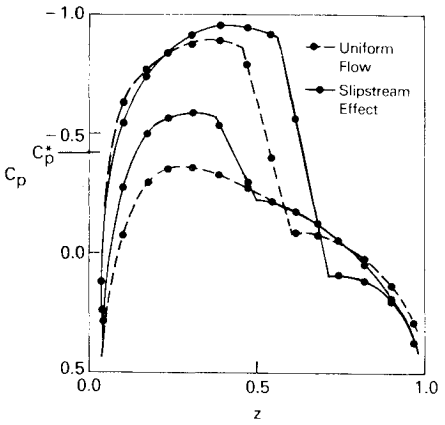

Fig. 5 C_p distribution at section A of wing.

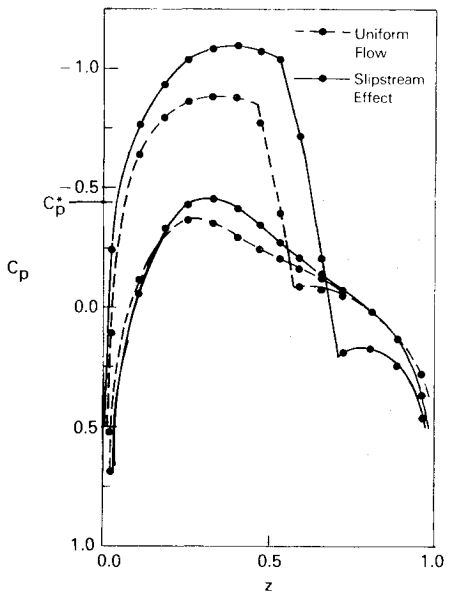

Fig. 6 C_p distribution at section B of wing.

$\alpha=\beta=1$, allowing the problem to be solved with no special treatment for points at the slipstream boundary. Although the application of Eqs. (15) and (16) is a simple matter in our present calculations where cylindrical coordinates are used, a more complex set of equations replaces them when general coordinate systems are used. In such cases a great simplification is caused by avoiding any special treatment for points at the slipstream boundary.

Profiles of the pressure coefficient

$$C_P=2(p-p_{o\infty})$$

at sections A and B of the wing (see Fig. 2) are given in Figs. 5 and 6. In these figures the symbols on the curves indicate the numerical solution obtained at the mesh points. At section A the swirl angle effectively reduces the wing's angle of attack. On the upper surface, the axial velocity increment in the slipstream and the swirl angle produce opposite effects. They, however, produce similar effects on the lower surface. The swirl angle tends to produce an upstream displacement in the upper surface shock position, while the axial velocity increment tends to produce a downstream displacement. At section B, the swirl angle effectively increases the wing's angle of attack. The axial velocity increment and the swirl angle produce similar effects on the wing's upper surface and opposite effects on its lower surface. We note in Fig. 6 that the slipstream effect produces a downstream displacement in the shock position, and it produces a stronger shock. This consequently contributes to an increase in the wave drag. Figures 7 and 8 show the distribution of C_{pmin} (the minimum value of C_p along a chord) along the wing span. In these figures we see that the slipstream effect is largest inside the slipstream, but extends outside it. Figure 9 shows the distribution along the wing span of c_l, the section lift coefficient. It is concluded from this figure that the slipstream effect on lift distribution is primarily due to the swirl angle. It is clear that rolling moments will occur due to the slipstream.

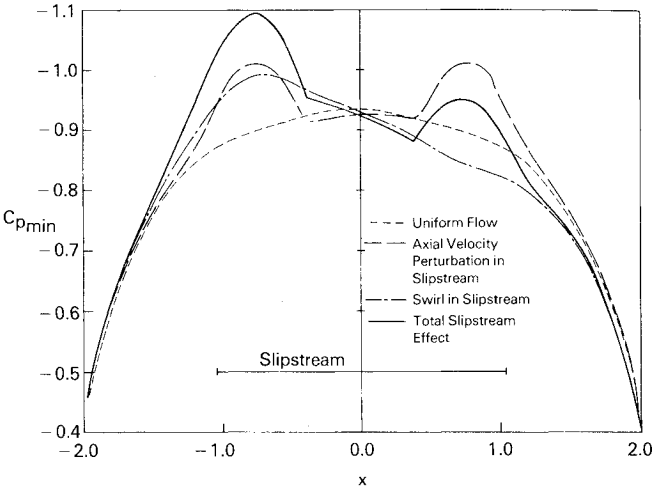

Fig. 7 Minimum C_p distribution along wing top.

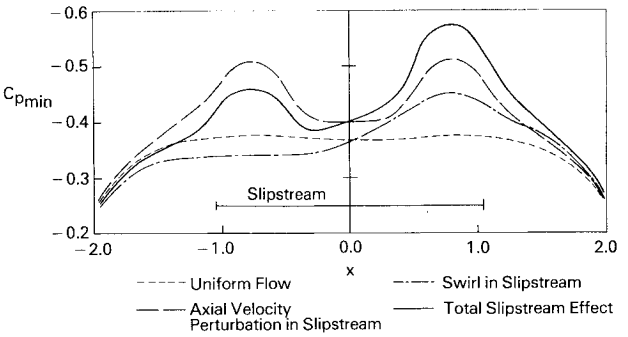

Fig. 8 Minimum C_p distribution along wing bottom.

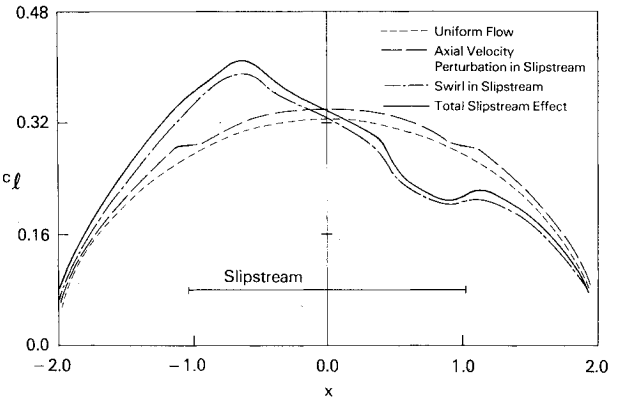

Fig. 9 Lift distribution for wing.

The effect of the slipstream on the wing's wave drag is shown in Table 1, where the left wing denotes the wing half which includes section B (see Fig. 2), and for which the slipstream swirl is in the upward direction, while the right wing denotes the wing half which includes section A and for which the slipstream swirl is in the downward direction.

Table 1 Normalized wave drag for rectangular wing

	Uniform flow	Slipstream axial velocity effect	Slipstream swirl effect	Combined effect
Right wing drag	1.00	2.83	0.68	2.04
Left wing drag	1.00	2.83	1.48	3.82
Total wing drag	2.00	5.66	2.16	5.86

Table 2 Normalized lift

	Uniform flow	Slipstream axial velocity effect	Slipstream swirl effect	Combined effect
Right wing lift	1.00	1.05	0.83	0.87
Left wing lift	1.00	1.05	1.17	1.23
Total wing lift	2.00	2.10	2.00	2.00

Estimates of wave drag are found[10] by integrating

$$\int_{\text{shock}} [\phi_z]^3 ds$$

where the integral is taken along shock waves and $[\phi_z]$ is the jump in ϕ_z across the shock. In Table 1 the drag is normalized by that drag due to the wing semispan in the absence of the slipstream. The table shows that the swirl effect on wave drag is that of redistribution. Its effect on the total wave drag however is small. This is in contrast to the slipstream axial velocity which produces a large increase in wave drag.

The effect of the slipstream on the wing's lift is shown in Table 2. Estimates of lift are found by integrating $\Delta\phi_{te}$ (the difference in ϕ between the upper and lower wing trailing-edge surfaces) along the wing span. The lift values shown in the table are normalized by that due to the wing semispan in the absence of the slipstream. Table 2 shows that the effect of the slipstream on the wing's total lift is minor.

Experimental results on the effects of propeller slipstreams on the aerodynamic properties of wings in the transonic regime are available only for complex test configurations. In Ref. 7 the interference effects were found for a wing-body configuration with a 32 deg swept, supercritical, tapered, cranked wing. An ejector-nacelle propeller slipstream simulator was used to produce a slipstream with characteristics typical of advanced propellers presently being investigated (see Figs. 3 and 4). The present work was conducted using a simple numerical code which does not allow the modeling of the complex test configuration used in that experiment. The blunt leading edge of the supercritical wing used in the experiment and the complex wing-body configuration require the use of complex, recently developed numerical techniques.[11]

A quantitative comparison between the experimental results and the numerical results is not appropriate due to differences in the geometrical configurations of the experimental and numerical test cases. However, a qualitative comparison in which points of similarity between the two sets of results are indicated and apparent discrepancies are explained is appropriate here. Comparisons are made below between the experimental results at a freestream Mach number of 0.8 and the numerical results presented above. In agreement with the present numerical calculations, the experimental results of Ref. 7 indicate that the slipstream effect on the wing's aerodynamic properties is mainly confined to that portion of the wing immersed in the slipstream. The experimental results for a maximum swirl angle $\alpha_{s\infty max} = 7$ deg indicate that aerodynamic effects due to swirl are more significant than those due to the axial velocity perturbation in the slipstream. The result indicated by the numerical calculations in Fig. 9 is in agreement with the above observation since the perturbation magnitude of the section lift coefficient due to swirl only is larger than the corresponding perturbation due to the axial velocity increment in the slipstream. Figures 7 and 8, however, indicate that the perturbation magnitude of $C_{p\min}$ along the wing span due to swirl is of the same order as the corresponding perturbation due to the axial velocity increment in the slipstream. The apparent discrepancy between the experimental results and the results indicated by Figs. 7 and 8 may be explained by noting that a value of 3 deg was used for $\alpha_{s\infty max}$, the maximum slipstream swirl angle in the numerical calculations, while the corresponding value in the experiment was 7 deg. Since the effect of swirl on the aerodynamic properties of the wing increases as the swirl angle $\alpha_{s\infty max}$ increases, the relatively weak effect of the slipstream swirl predicted by the numerical calculations is expected. The experimental results show that lift coefficient increments due to the slipstream are small and are on the order of 4% of the wing-body lift. This result is in the same range as that indicated by the numerical calculations (see Table 2). The experimental results show that the incremental drag due to the slipstream depends on the swirl angle $\alpha_{s\infty max}$. It is 3% of the wing-body drag for $\alpha_{s\infty max} = 7$ deg and it is -3% for $\alpha_{s\infty max} = 11$ deg. The drag reduction in the second case is due to the induced drag. The numerical calculations presented here have indicated that the incremental wave drag due to the slipstream is approximately 200% of the wave drag in the absence of the slipstream. Since the experimental drag is the total drag and no estimate of the individual drag components (wave, induced, and viscous) was made, it is not possible to make a meaningful comparison between the experimental and the numerical drag results.

It is worth noting here the slipstream effects which are characteristic of the transonic regime. The slipstream swirl effectively increases the angle of attack on the upgoing side of the slipstream and therefore increases the shock strength there. The axial velocity increment in the slipstream increases the Mach number there over the freestream value and therefore causes an increase in the shock strength. In addition to the increased wave drag resulting from the stronger shock waves, boundary-layer separation may occur, affecting the lift. Due to the effects the slipstream has on shock waves and the possible adverse effects these may cause to the wing aerodynamic properties, it is necessary to obtain a good understanding of the effects of slipstreams on wings and to design wings properly to avoid the adverse effects. The analyses and design done to date for wings interacting with slipstreams in the transonic regime have employed panel methods which fail to handle supersonic patches and shock waves correctly. The method presented in this work for calculating the aerodynamic effects of nearly uniform slipstreams on thin wings overcomes the deficiencies of panel

methods. Moreover, it allows us to obtain information about a rotational flow problem by solving a potential equation. This equation was arrived at by making reasonable approximations in the Euler equations consistent with the physical problem under consideration. The other alternative of solving the Euler equations is not an attractive one, since these have the disadvantages of complexity, large computer storage requirements, and long computational time.

Conclusion

In this paper we have presented an inviscid model for the interaction between a thin wing and a nearly uniform propeller slipstream. In this model the perturbation velocities due to the interaction are potential even though the undisturbed slipstream velocity is rotational. This allows us to obtain basic information about the interaction problem while avoiding the need for solving the Euler equations. For typical slipstream velocity distributions, only minor modifications to the free flow potential equation and wing boundary conditions are required to produce the slipstream effect.

The slipstream effect on a wing in the transonic regime has been demonstrated through a simple example. Solutions obtained for a rectangular wing indicate that the slipstream has a strong effect on the aerodynamic properties of the wing portion immersed in the slipstream. The effect of the slipstream on the rest of the wing is less, but it is discernable. The results indicate that the slipstream swirl has a strong effect on the wing load distribution, producing rolling moments; however, its effect on the total wing lift and wave drag is small. The axial velocity increment inside the slipstream has little effect on the wing's lift; however, it causes a large increase in wave drag due to increased shock wave strength.

The results presented indicate the basic characteristics of the slipstream/wing interaction problem. The results are in qualitative agreement with the limited experimental results available; however, the lack of data for simple geometric configurations has severely restricted comparison with experiments. More detailed calculations are required to evaluate the present approach further. Even though the present approach to the interaction problem was applied to a geometrically simple test case and the equation solved was the potential small-disturbance equation, the same approach may be used to solve problems of geometrically complex nature, and problems which require the use of the full-potential equation, provided the basic assumptions are not violated. The approach presented here is preferable to the use of Euler equations which have the disadvantage of complexity, large computer storage requirements, and long computational time. The approach presented here overcomes the major deficiency of the panel method—which is its failure to predict correct solutions in supersonic patches and at shock waves. Due to the effects the slipstream has on shock waves and the possible adverse effects these may cause to the wing aerodynamic properties, it is of utmost importance to model the shocks correctly in slipstream/wing interaction studies for the transonic range.

Acknowledgments

The author would like to thank M. Hafez for many valuable discussions. This work was sponsored by NASA Ames under Contract NAS2-9913.

References

[1] Shollenberger, C. A., "Three-Dimensional Wing/Jet Interaction Analysis Including Jet Distortion Influences," *Journal of Aircraft,* Vol. 12, Sept. 1975, pp. 706-713.

[2] Lan, C.E., "Wing-Slipstream Interaction with Mach Number Nonuniformity," *Journal of Aircraft,* Vol. 12, Oct. 1975, pp. 759-760.

[3] Ting, L., Liu, C.H., and Kleinstein, G., "Interference of Wing and Multipropellers," *AIAA Journal,* Vol. 10, July 1972, pp. 906-914.

[4] Chow, F., Krause, E., Liu, C.H., and Mao, J., "Numerical Investigations of an Airfoil in a Nonuniform Stream," *Journal of Aircraft,* Vol. 7, Nov.-Dec. 1970, pp. 531-537.

[5] Kleinstein, G. and Liu, C.H., "Application of Airfoil Theory for Nonuniform Streams to Wing Propeller Interaction," *Journal of Aircraft,* Vol. 9, Feb. 1972, pp. 137-142.

[6] Boctor, M. L., Clay, C.W., and Watson, C.F., "An Analysis of Prop-Fan/Airframe Aerodynamic Integration," NASA CR-152186, 1978.

[7] Welge, H.R. and Crowder, J.P., "Simulated Propeller Slipstream Effects on a Supercritical Wing," NASA CR-152138, 1978.

[8] Jameson, A., "Numerical Computation of Transonic Flows with Shock Waves," *Symposium Transsonicum II,* Springer-Verlag, New York, 1976, pp. 384-414.

[9] Hafez, M.M., Murman, E.M., and South, J.C., "Artificial Compressibility Methods for Numerical Solution of Transonic Full Potential Equation," AIAA Paper 78-1148, 11th Fluid Dynamics Conference, Seattle, Wash., July 1978.

[10] Murman, E.M. and Cole, J.D., "Inviscid Drag at Transonic Speeds," AIAA Paper 74-540, 7th Fluid and Plasma Dynamics Conference, Palo Alto, Calif., June 1974.

[11] Caughey, D.A. and Jameson, A., "Recent Progress in Finite-Volume Calculations for Wing-Fuselage Combinations," AIAA Paper 79-1513, 12th Fluid and Plasma Dynamics Conference, Williamsburg, Va., July 1979.